Academic Journal of Engineering and Technology Science
ISSN 2616-5667 Vol.3, Issue 3: 95-103, DOI: 10.25236/AJETS.2020.030312

Study on the Influence of Material Parameters on Indentation Morphology

Wenjie Qian, Jianguo Zhu*

Faculty of Civil Engineering and Mechanics, Jiangsu University, Zhenjiang 212013, Jiangsu, China
Corresponding author e-mail: zhejiujiyi@outlook.com

ABSTRACT. *In the process of metal welding, residual stress will inevitably be introduced. In the real service environment, the residual stress will also undergo further evolution and development, which will directly affect the properties of materials or components, and then threaten the safety of life and property. Therefore, it is of great practical value to study the rapid and accurate measurement method of residual stress. Traditional test methods have their limitations, thus, someone proposed that the magnitude and direction of residual stress can be characterized based on the morphology after unloading of spherical indentation. But the effect of material parameters on the pile-up morphology has not been studied. In this paper, the influence of material parameters on the indentation morphology is systematically studied by finite element simulation. The research results show that materials with a hardening index greater than 0.3 are not recommended to use this method, and the yield strength has little effect on the results.*

KEYWORDS: *residual stress, indentation, finite element method, material parameter*

1. Introduction

In the construction industry, the proportion of steel structures is already as high as 60%. During the construction of the steel structure, it is necessary to connect the steel by welding technology to obtain a stable connection joint. However, the metal material will produce residual stress in the welding structure due to deformation during welding, and at the same time, the residual stress inside the component will evolve and develop continuously during the service process of the component [1, 2]. The existence of welding residual stress will have a great influence on the mechanical properties of the component, which will directly affect the mechanical properties such as fatigue strength, crack strength and corrosion resistance of the component, which may lead to deformation or even sudden cracking of the component, and then cause the failure of the whole structure [3, 4]. Therefore, to promote the better application of metal materials in the engineering field, it will be of great engineering practical significance to systematically study the accurate measurement method of welding residual stress.

ISSN 2616-5667 Vol.3, Issue 3: 95-103, DOI: 10.25236/AJETS.2020.030312

The traditional residual stress testing methods mainly include the physical method and mechanical method. Generally, the physical methods [5–7] include the X-ray diffraction, neutron diffraction, and ultrasonic wave techniques, while the mechanical methods [8–11] include the hole-drilling, slitting and ring-core cutting techniques. However, these methods have their limitations, so Shen et al. [12–14] proposed that the magnitude and direction of residual stress can be characterized based on the morphology after the unloading of spherical indentation. The method is simple to measure, and the magnitude and direction of residual stress can be determined simultaneously by one measurement. However, this method is affected by many factors. For instance, the parameters of the material itself will have a great influence on the measurement results. Therefore, it is necessary to carry out a study on the relationship between parameters and pile-up morphology.

In this paper, the material parameters related to the pile-up morphology are determined by dimensionless analysis. Then, the influence of material parameters on the indentation morphology is systematically studied by finite element simulation. Finally, the influence of residual stress on the indentation morphology is studied.

2. Dimensionless analysis

The dimensionless analysis is a simple method to determine material parameters [15]. The dimensionless function was established through the parametric FEM study which can correlate the indentation curve with the parameters to be identified. Thus, we can know which parameters are worth studying by dimensionless analysis.

For the specimens under spherical indentation with residual stress, the loading F is considered to be a function of the following parameters: the Elastic modulus, E, Poisson's ratio, v, yield strength, σ_y, work hardening exponent, n, indenter tip radius, R, the maximum depth, h, and surface residual stress, σ_R. It can be expressed as follows:

$$F = f\left(E, v, \sigma_y, n, R, h, \sigma^R\right) \tag{1}$$

In this study, E and R are selected as the basic variables, and the following dimensionless function can be obtained by using Π theory in dimensional analysis.

$$F = ER^2\Pi_1\left(v, \frac{\sigma_y}{E}, n, \frac{h}{R}; \frac{\sigma_R}{E}\right) \tag{2}$$

Replace the dimensionless σ_R/E with σ_R/σ_y, we can obtain

$$F = ER^2\Pi_1\left(v, \frac{\sigma_y}{E}, n, \frac{h}{R}; \frac{\sigma_R}{\sigma_y}\right) \tag{3}$$

Similarly, for the specimens under spherical indentation without residual stress, the loading F_0 can be expressed as

ISSN 2616-5667 Vol.3, Issue 3: 95-103, DOI: 10.25236/AJETS.2020.030312

$$F_0 = f\left(E, v, \sigma_y, n, R, h\right) \tag{4}$$

Select the E and h as the basic variables, another dimensionless function which can be obtained by using Π theory was as follows:

$$F_0 = ER^2\Pi_0\left(v, \frac{\sigma_y}{E}, n, \frac{h}{R}\right) \tag{5}$$

From Eqs. (3) and (5), the relative change of load between stressed and unstressed samples, $(F\text{-}F_0)/F_0$, is given by

$$\frac{F-F_0}{F_0} = \frac{\Pi_1\left(v, \frac{\sigma_y}{E}, n, \frac{h}{R}; \frac{\sigma_R}{\sigma_y}\right) - \Pi_0\left(v, \frac{\sigma_y}{E}, n, \frac{h}{R}\right)}{\Pi_0\left(v, \frac{\sigma_y}{E}, n, \frac{h}{R}\right)} = \Pi\left(v, \frac{\sigma_y}{E}, n, \frac{h}{R}; \frac{\sigma_R}{\sigma_y}\right) \tag{6}$$

Considering that the simulation adopts the method of fixed indentation depth, h, the parameters such as the diameter of the indenter tip radius, R, have been determined, and the yield strain $\varepsilon_y = \sigma_y/E$. Thus, the above equation can be simplified into the following equation.

$$\frac{F-F_0}{F_0}\Big|_{h/R=0.1} = \Pi\left(\varepsilon_y, n, \frac{\sigma_R}{\sigma_y}\right) \tag{7}$$

Due to dimensionless function is only related to ε_y, n, and σ_R. Thus, only these three material parameters are considered in the subsequent simulation

3. Numerical models and basic assumptions

Elastic/plastic indentation was simulated using the conical indentation and spherical indentation by the ABAQUS 6.14, respectively. Two models were established, the difference of which was that the shape of the indenter was different, while the other model parameters were identical. The indenter was modeled as an analytical rigid body with a semi-angle ϕ=70.3° for conical indenter, while the indenter tip radius is 1.25 mm for spherical indenter. Due to the symmetry of the indentation model, a two-dimensional axisymmetry model can be used to simplify the three-dimensional problem.

All simulations were performed to a depth of 0.3 mm and then withdrawing using the finite element mesh and boundary conditions illustrated in Figure 1, in which the specimen is modeled as a cylinder 10 mm high and 10 nm in radius by 11141 four-node axisymmetric elements while the mesh properties are defined as CAX4R due to its high computational accuracy and are suitability for large strain analysis. Roller boundary conditions were applied along the axis of symmetry and the bottom surface separately, a free surface was modeled at the outside of the

ISSN 2616-5667 Vol.3, Issue 3: 95-103, DOI: 10.25236/AJETS.2020.030312

cylinder, and the interface between the indenter and the specimen was assumed to be frictionless. Figure 2 shows details of the finite element mesh in the region of the specimen near the tip of the indenter. Due to a large local deformation that may occur near the indentation area, thus, a very fine mesh is needed in the contact region to obtain accurate simulation. Correspondingly, a progressively coarser mesh was employed far away from the contact area.

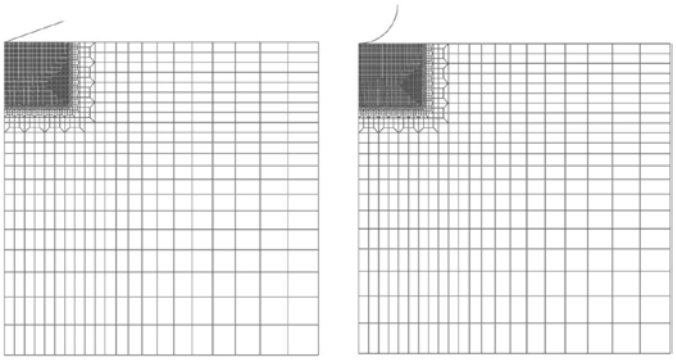

Figure. 1 The finite element mesh of conical indentation and spherical indentation

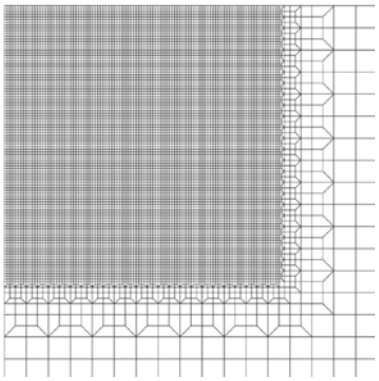

Figure. 2 Details of the finite element mesh near the indentation area

During the simulation, the elastic modulus of the material is assumed to be 71GPa and the Poisson's ratio is 0.3. In the simulation of loading and unloading, displacement loading was adopted to control the loading and unloading process. Materials with different E/σ_y ratios from 100 to 1000 were investigated by varying the yield stress. Additionally, the work hardening exponent, n, has also been varied from 0.1 to 0.5. Two different surface residual stresses were applied to the model for the investigation of effect from residual stress as well. It is should be pointed out that the minus sign indicates compression.

ISSN 2616-5667 Vol.3, Issue 3: 95-103, DOI: 10.25236/AJETS.2020.030312

4. Results and discussion

Before studying the applicability of the two indentation modes, the qualitatively study for the influence of material parameter changes on the results of the two indentation modes by changing the material parameters can be meaningful. The change of material parameters can simulate most of the material states. Thus, the sensitivity of the data obtained under the two indentation modes to different material parameters can be studied.

Figure 3 shows the contact area ratio varies with work hardening exponent and yield strength under sharp and spherical indentation, respectively. In the figure, the sharp indentation is represented by a solid line and the *C* is represented by conical indenter while the spherical indentation is represented by the dotted line and the *S* is represented by spherical indenter, and the A_c represents the real contact area obtained by ABAQUS while the A_g represents the theoretical contact area obtained by geometrical relationship. Additionally, the contact area ratio A_c/A_g was used to represents the change in contact area due to the theoretical contact area of different indenter is different, thus, it is not suitable to compare the real contact area of the two indenters directly, and contact area ratio A_c/A_g of the two indenters can be used for comparison.

Figure 3(a) shows that the contact area ratio of both sharp and spherical indentation was decreased with the increase of work hardening exponent, and the contact area ratio of spherical indentation was always greater than sharp indentation applied the same biaxial stresses. This result indicates that with the increase of material work hardening exponent, the pile-up will be decreased, so its maximum contact area will be decreased accordingly. Additionally, this result shows that the pile-up of spherical indentation could be greater than sharp indentation, so the contact area ratio of spherical indentation was always greater than sharp indentation. Figure 3(b) shows that that the contact area ratio of both sharp and spherical indentation was increased with the increase of E/σ_y, which means with the decrease of σ_y, the pile-up will be increased, thus, the maximum contact area will be increased accordingly. And the contact area ratio of spherical indentation was always greater than sharp indentation applied the same biaxial stresses indicates that the pile-up of spherical indentation could be greater than sharp indentation which similar to the results of varying the work hardening exponent. Figure 4 shows the maximum pile-up varies with work hardening exponent and yield strength, and the results in Figure 4 validates the interpretation of Figure 3. It should be pointed out that the applied biaxial stresses have a significant influence on the contact area and pile-up in Figure 3 and Figure 4. The compression stress can increase the contact area and the pile-up while the tension stress can decrease the contact area and the pile-up under both sharp and spherical indentation.

ISSN 2616-5667 Vol.3, Issue 3: 95-103, DOI: 10.25236/AJETS.2020.030312

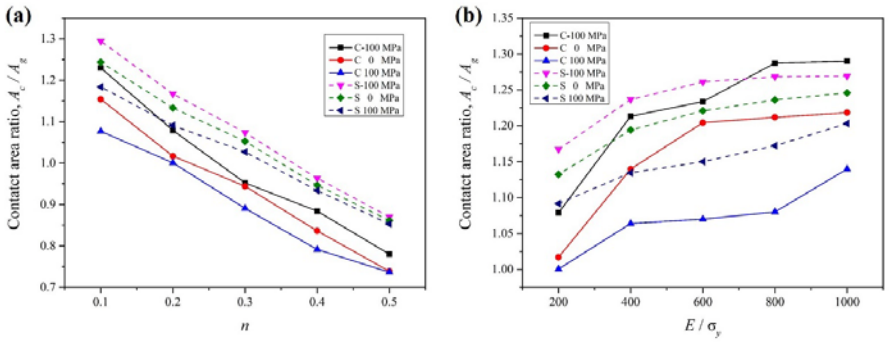

Figure. 3 The contact area ratio vary with work hardening exponent and yield strength : (a) n, and (b) E/σy

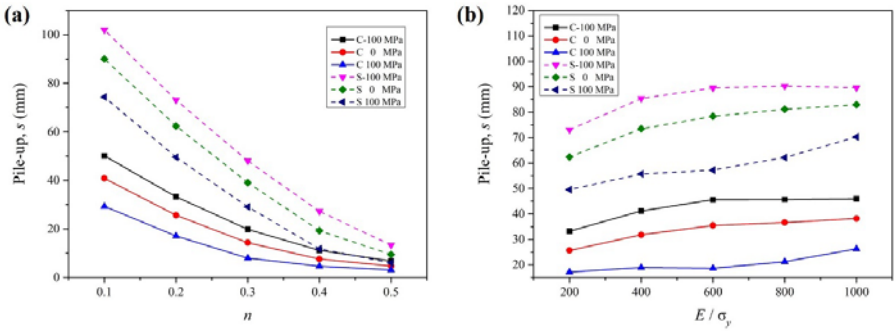

Figure. 4 The maximum pile-up vary with work hardening exponent and yield strength : (a) n, and (b) E/σy

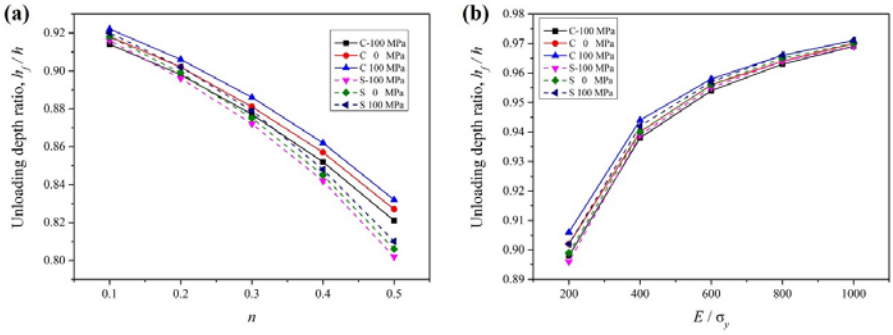

Figure. 5 The unloading depth ratio vary with work hardening exponent and yield strength : (a) n, and (b) E/σy

ISSN 2616-5667 Vol.3, Issue 3: 95-103, DOI: 10.25236/AJETS.2020.030312

Figure 5 shows the unloading depth ratio varies with work hardening exponent and yield strength, and the h_f and h in the figure represent the unloading depth and the maximum indentation depth, respectively. In the simulation, the maximum indentation depth h was determined to be 0.3 mm, and the unloading depth h_f was obtained from load-displacement curves.

Figure 5(a) shows that the unloading depth ratio of both sharp and spherical indentation was decreased with the increase of work hardening exponent, and the unloading depth ratio of spherical indentation was always less than sharp indentation applied the same biaxial stresses. This result indicates that with the increase of material work hardening exponent, the elastic recovery will be increased, so its unloading depth will be decreased accordingly. Additionally, this result shows that the elastic recovery of spherical indentation could be greater than sharp indentation, so the unloading depth spherical indentation was always less than sharp indentation. Figure 3(b) shows that that the unloading depth ratio of both sharp and spherical indentation was increased with the increase of E/σ_y, which means with the decrease of σ_y, the elastic recovery will be decreased, thus, the unloading depth will be increased accordingly. And the unloading depth ratio of spherical indentation was always less than sharp indentation applied the same biaxial stresses indicates that the elastic recovery of spherical indentation could be greater than sharp indentation which similar to the results of varying the work hardening exponent. And it can be seen from Figure 5 that the compression stress can decrease the unloading depth while the tension stress can increase the unloading depth under both sharp and spherical indentation, which means the compression stress can increase the elastic recovery while the tension stress can decrease the elastic recovery.

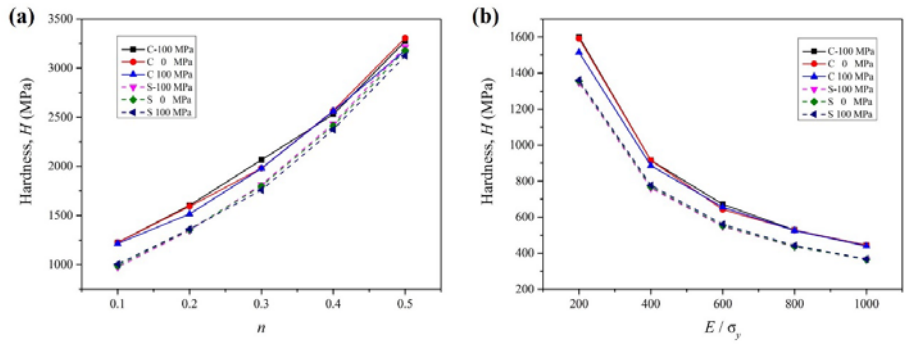

Figure 6. The calculated hardness varies with work hardening exponent and yield strength : (a) n, and (b) E/σy

Figure 6 is based on the calculation formula for hardness to calculate the variation of material hardness with work hardening index and yield strength. As can be seen from Figure 6(a), the hardness of both conical and spherical indentation increases with the increase of work hardening index under the same residual stress. From Figure 6(b), it can be seen that the calculated hardness of both cone and sphere

ISSN 2616-5667 Vol.3, Issue 3: 95-103, DOI: 10.25236/AJETS.2020.030312

decreases with the increase of E/σy under the same residual stress, which may be due to the decrease of the hardness of the material as the σy decreases. Besides, when the same indenter is used, the applied residual stress has little effect on the hardness of the material, which is the same as the conclusion of the published literature.

5. Conclusion

By analyzing the influence of material parameters on the indentation morphology response, it is found that for both indentation modes, the hardening index and yield strength will affect the pile-up morphology, contact area, unloading depth, and material hardness. For the pile-up morphology, the results show that the hardening index has the most obvious effect on it. At a high hardening index, the difference of pile-up height in different stress states is very small, while at low hardening index, the difference of pile-up height in different stress states is very obvious. Simulation analysis based on this study found that materials with a hardening index greater than 0.3 are not recommended to use this method. Besides, the results of yield strength show that these material parameters have little effect on the results.

Acknowledgments

The authors are grateful for the financial support from the National Natural Science Foundation of China (Grant nos. 11672345, 11872025), the Natural Science Foundation of Jiangsu Province (Grant nos. BK20161341, BK20170518), the Six Talent Peaks Project in Jiangsu Province (Grant no. 2016-HKHT-004) and the Postgraduate Research & Practice Innovation Program of Jiangsu Province (KYCX19_1579).

References

[1] Yang YC, Chang E. Influence of residual stress on bonding strength and fracture of plasma-sprayed hydroxyapatite coatings on Ti-6Al-4V substrate. Biomaterials 2001; 22: 1827–36.
[2] Laamouri A, Sidhom H, Braham C. Evaluation of residual stress relaxation and its effect on fatigue strength of AISI 316L stainless steel ground surfaces: Experimental and numerical approaches. Int J Fatigue 2013; 48: 109–21.
[3] Toribio J. Residual Stress Effects in Stress-Corrosion Cracking. J Mater Eng Perform 1998; 7: 173–82.
[4] Mao WG, Wan J, Dai CY, Ding J, Zhang Y, Zhou YC, et al. Evaluation of microhardness, fracture toughness and residual stress in a thermal barrier coating system: A modified Vickers indentation technique. Surf Coatings Technol 2012; 206: 4455–61.

ISSN 2616-5667 Vol.3, Issue 3: 95-103, DOI: 10.25236/AJETS.2020.030312

[5] Mahmoodi M, Sedighi M, Tanner DA. Investigation of through thickness residual stress distribution in equal channel angular rolled Al 5083 alloy by layer removal technique and X-ray diffraction. Mater Des 2012; 40: 516–20.
[6] Hu E, He Y, Chen Y. Experimental study on the surface stress measurement with Rayleigh wave detection technique. Appl Acoust 2009; 70: 356–60.
[7] Gauthier J, Krause TW, Atherton DL. Measurement of residual stress in steel using the magnetic Barkhausen noise technique. NDT E Int 1998; 31: 23–31.
[8] Mainjot AK, Schajer GS, Vanheusden AJ, Sadoun MJ. Residual stress measurement in veneering ceramic by hole-drilling. Dent Mater 2011; 27: 439–44.
[9] Montay G, Cherouat A, Lu J, Baradel N, Bianchi L. Development of the high-precision incremental-step hole-drilling method for the study of residual stress in multi-layer materials: Influence of temperature and substrate on ZrO2-Y2O3 8 wt% coatings. Surf Coatings Technol 2002; 155: 152–60.
[10] Cheng W, Iain Finnie. Residual Stress Measurement and the Slitting Method.
[11] Masláková K, Trebuňa F, Frankovský P, Binda M. Applications of the strain gauge for determination of residual stresses using Ring-core method. Procedia
[12] Lu Z, Feng Y, Peng G, Yang R, Huan Y, Zhang T. Estimation of surface equi-biaxial residual stress by using instrumented sharp indentation. Mater Sci Eng A 2014; 614: 264–72.
[13] Shen L, He Y, Liu D, Wang M, Lei J. Prediction of residual stress components and their directions from pile-up morphology: An experimental study. J Mater Res 2016; 31: 2392–7.
[14] Peng G, Feng Y, Huan Y, Zhang T, Ma Y, Lu Z. Spherical indentation method for estimating equibiaxial residual stress and elastic–plastic properties of metals simultaneously. J Mater Res 2018; 33: 884–97.
[15] Cheng YT, Cheng CM. Scaling, dimensional analysis, and indentation measurements. Mater Sci Eng R Reports 2004; 44: 91–149.